Journal of Innovative Optical Health Sciences
Vol. 1, No. 1 (2008) 17–28

World Scientific
www.worldscientific.com

QUANTITATIVE EVALUATION OF RETINAL TUMOR VOLUME IN MOUSE MODEL OF RETINOBLASTOMA BY USING ULTRA HIGH-RESOLUTION OPTICAL COHERENCE TOMOGRAPHY

MARCO RUGGERI*, HASSAN WEHBE*, GAVRIIL TSECHPENAKIS†,
SHULIANG JIAO*,‡, MARIA ELENA JOCKOVICH*,
COLLEEN CEBULLA*, ELEUT HERNANDEZ*,
TIMOTHY G. MURRAY* and CARMEN A. PULIAFITO*

*Bascom Palmer Eye Institute
University of Miami Miller School of Medicine
1638 NW 10th Ave. Miami, FL 33136, USA
‡sjiao@med.miami.edu

†Electrical and Computer Engineering Department
University of Miami, 1251 Memorial Dr
Coral Gables, FL 33124, USA

An ultra high resolution spectral-domain optical coherence tomography (SD-OCT) together with an advanced animal restraint and positioning system was built for noninvasive non-contact *in vivo* three-dimensional imaging of rodent models of ocular diseases. The animal positioning system allowed the operator to rapidly locate and switch the areas of interest on the retina. This function together with the capability of precise spatial registration provided by the generated OCT fundus image allows the system to locate and compare the same lesion (retinal tumor in the current study) at different time point throughout the entire course of the disease progression. An algorithm for fully automatic segmentation of the tumor boundaries and calculation of tumor volume was developed. The system and algorithm were successfully applied to monitoring retinal tumor growth quantitatively over time in the $LH_{BETA}T_{AG}$ mouse model of retinoblastoma.

Keywords: 3D imaging; retina; mouse models; optical coherence tomography; image segmentation.

1. Introduction

Retinoblastoma is a form of cancer affecting the light-sensitive retinal cells that enables sight. The disease is the most common ocular malignancy in children, occurring approximately in one of every 15,000 births.[1,2] Over the last century, significant advances in screening and treatment have led to virtually all children being cured of the primary eye cancer. However, serious concerns exist regarding the significant

‡Corresponding author.

morbidity and potential mortality associated with current therapies, therefore new therapeutic modalities are investigated. *In vivo* assessment of the structural and morphological changes of the retina at different stages is essential in monitoring the disease progression and the response to treatments. Histology is at present the standard method for quantitative examination of the retinal morphology and anatomy of small animals. As a result, a large number of animals must be sacrificed to achieve a statistically significant experimental result, and each animal contributes to just a single data point for a study. Noninvasive *in vivo* examination of the animal retina allows the monitoring of disease progression through its entire course in individual animals and provides a better understanding of the pathophysiology of the disease.

Imaging the retina of mouse is challenging due to the small size of the eye and the pupil, which make the alignment for light delivery into the eye formidable. Other challenges in longitudinal studies in mouse models are to image the same area of the retina repeatedly over time and to search the lesions (areas of interest) at the beginning of a study cycle. For example, there may be multiple tumors in the retina of a $LH_{BETA}T_{AG}$ mouse (a model of retinoblastoma), usually originating at the edge of the retina, and frequently a single raster OCT (optical coherence tomography) scan can not capture all of them. To capture the tumors the eye must be tilted at a large angle so that the incident sample light can reach the edge of the retina, and the entire retina needs to be screened with multiple partially overlapped raster scans.

As a high resolution noninvasive imaging modality, OCT[3,4] has been applied to mouse retinal imaging[5–11] with various degrees of success. In a previous paper we reported the development of a spectral-domain OCT (SD-OCT) prototype for high resolution imaging of rodent retina. Among all the previous successful applications, the retinal tumor of a retinoblastoma mouse model was successfully imaged for the first time *in vivo*. More importantly, the tumor volume was calculated by using manual segmentation of the tumor boundaries in the OCT images. As an effort to further improve the imaging quality and throughput, a novel animal positioning system together with an ultra-high resolution SD-OCT system were developed. The system was tested on imaging mouse and rat retina, especially retinal tumor in a mouse model. We also developed an algorithm for fully automatic segmentation of the tumor boundaries and calculation of the tumor volume. The system was applied in monitoring retinal tumor growth on the $LH_{BETA}T_{AG}$ transgenic mouse model of retinoblastoma.[12] The technology provides a high throughput quantitative noninvasive imaging tool, which will facilitate the study of the pathogenesis and new therapies for this malignant disease on mouse model.

2. Material and Methods

2.1. *Ultra high resolution OCT imaging system*

The configuration of the OCT and the optical delivery system in the sample arm are similar to those reported before except that the optical components were modified to accommodate broader bandwidth. A three-module superluminescent diode

(SLD) (Broadlighter, T840-HP, Superlumdiodes Ltd, Moscow Russia) with a center wavelength of 840 nm and a FWHM (full width at half maximum) bandwidth of 100 nm was used. The light source provided a low coherence light at a power of 15 mW exiting the single mode optical fiber pigtail. The low coherence light was coupled into a fiber based Michelson interferometer that consist of a 2×2 3 dB fiber coupler, which split the light into the reference arm and the sample arm. The sample light was delivered to a modified optical head of an OCT 2 system (Carl Zeiss Meditec Inc. Dublin, CA), which consisted of a X–Y galvanometer optical scanner and the optics for delivering the sample light into the rodent retina and collecting the backreflected sample light. A double-aspheric 90D Volk lens (Volk Optics Inc., OH) was used as the objective lens. The power of the sample light was lowered to 750 μW by adjusting the source power with a fiber-based pigtail style attenuator to ensure that the light intensity delivered to the eye was safe to the retina. In the detection arm, a spectrometer consisting of a collimating lens ($f = 50$ mm), a 1200 line/mm transmission grating, an achromatic imaging lens ($f = 180$ mm), and a line scan CCD camera (Aviiva-M2-CL-2014, 2048 pixels with 14 micron pixel size operating in 12-bit mode) was used to detect the combined reference and sample light. The calculated spectral resolution was 0.055 nm, which corresponds to a detectable depth range of 3.1 mm in air. An image acquisition board acquired the image captured by the CCD camera and transferred it to a computer workstation (IBM IntelliStation Z Pro, dual 3.6 GHz processor, 3 GB memory) for signal processing and image display. A complete raster scan consisting of 65536 scanning steps took about 2.7 seconds when the A-line (depth scan) rate of the OCT system was set to be 24 kHz. At this operating condition, the measured sensitivity was about 95 dB. The calibrated axial resolution of the system was $\sim$4 μm in the air corresponding to $\sim$3 μm in the tissue (the refractive index of the retina is $\sim$1.35). To calculate the scanning range of the OCT image we assumed the dioptric power of the mouse lens at wavelength of 840 nm (the center wavelength of the OCT system) to be 550D. This value was obtained by extrapolation from the published data of Remtulla *et al.*[13] The mechanical scan range at the scanners was set to 3° (optical scan range is 6°), which allowed to image an estimated area of 1×1 mm^2 on the mouse fundus and 2×2 mm^2 on the rat fundus.

2.2. *Animal positioning system and the experimental animal model*

The animal positioning system is important for high throughput applications, especially when a specific area of the retina has to be imaged over time. The main problem of a conventional multi-axis animal positioning system is that the axes for the rotations of the subject may not intersect and coincide with the pupil of the animal eye. As a result, a generic rotation of the animal may correspond to a change of the eye position in all directions and make the OCT image of the retina easily out of the field of view. It makes the alignment process even more formidable when the area of interest is far away from the optic disc as in the case of imaging

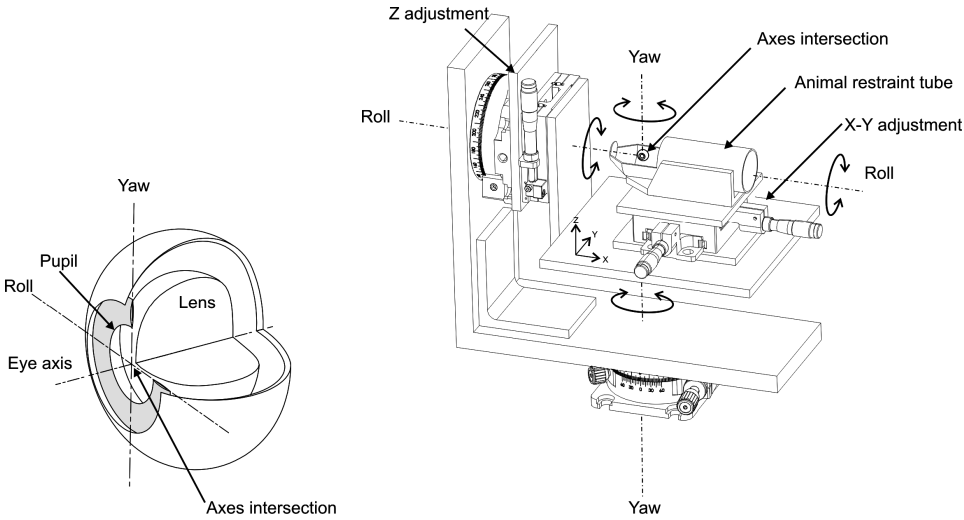

Fig. 1. (A) Concept of the two axis gimbal system for small animal retinal imaging. The pupil is positioned at the intersection of the rotational axes which is fixed in the space; (B) The design of the advanced animal positioning system. The system features 5-degrees of freedom: two rotational (yaw and roll) and three translational (X, Y, and Z).

the mouse model of retinoblastoma. We have developed an animal positioning system using the concept of gimbal systems in which the two orthogonal rotation axes (yaw and roll) intersect at the pupil of the animal eye (Fig. 1A). When the pivotal point of the scanned sample light coincides with the center of the pupil, rotation of the animal around any axis will only change the scanning area on the retina. A schematic of the design of the advanced animal positioning system is shown in Fig. 1B. The system features 5-degrees of freedom: two rotational (yaw and roll) and three translational (X, Y, and Z). The intersection of the two rotational axes is fixed in the space. By adjusting the animal using the three translational movements the position of the pupil can be set at the intersection of the rotational axes. The accuracy of rotation is 15 arcseconds, which corresponds to a lateral accuracy of about $0.13\,\mu$m on the mouse retina. The rotational ranges are greater than $\pm 20°$, which corresponds to about ± 1.3 mm on the retina. A removable animal restraint tube was built which allows easy insertion of the animal into the positioning system.

$LH_{BETA}T_{AG}$ mice[12] between weeks 10 and 14 were used for the experiments. In this model, tumor appears at 4 weeks of age and fills the available orbit volume by 16 weeks of age. A mouse from the same strain but free of tumor was used to characterize the positioning system. Animals were anesthetized 10 minutes before the experiments with a cocktail of Ketamine (80 mg/kg body weight) and Xylazine (10 mg/kg body weight) administered intramuscularly. In the meantime, the pupils were dilated with 10% Phenylephrine solution. Drops of balanced saline solution

were applied to the eyes to avoid dehydration of the cornea. After the animal was placed on the positioning system the fundus camera in the optical delivery system was used to guide the initial alignment to ensure the sample light was delivered through the dilated pupil. The final alignment was guided by monitoring and optimizing the real-time OCT image of the retina. Three OCT images at the upper, middle and bottom of the scanned area were displayed simultaneously in the real-time display for assisting the alignment. By monitoring the real-time OCT images and adjusting the gimbal animal positioning system the scanning area can be adjusted to cover the area of interest. In longitudinal studies the scanning area was verified by comparing the OCT fundus images generated from the measured raw OCT[14] data taken at different time points.

2.3. *Automatic segmentation of the boundaries of retinal tumors*

One significant parameter in evaluating the progression of the disease in retinoblastoma mouse models is the volume of the tumor mass. To calculate the tumor volume, segmentation of the tumor boundary accurately and reliably is the key, which is challenging because of the low contrast of the tumor image and the presence of speckle noise.

Here, we describe the algorithms we have developed for automatic segmentation of the tumor boundaries in each OCT B-scan. Although there is a lack of edges that can be used to determine the boundaries of different regions in the OCT images, texture is clearly the feature that can be used for the discrimination. However, the texture difference between the tumor and its surrounding regions (the background) cannot be easily captured. We have developed an approach[15–17] where an implicitly defined deformable model is driven by a discriminative Conditional Random Field (CRF), in a simple graphical probabilistic scheme. Thus, we solved the tumor segmentation problem as a topology independent maximum a posteriori probability (MAP) problem.[15] The main advantage of our approach is that it can capture local texture variations, since it updates the tumor statistics during the model evolution: in each iteration of the MAP estimation procedure, the newly detected tumor pixels/regions contribute with new information about the tumor texture. Our recent work[15–17] has shown that this approach can provide the desired accuracy in OCT image segmentation.

Let M be the deformable model, i.e., the evolving front that separates the tumor (model interior) R_M from the background $\Omega \backslash R_M$, where Ω indicates the image domain. We represent the model shape implicitly with the distance function

$$\Phi_M(\mathbf{x}) = \begin{cases} 0, & \mathbf{x} \in M \\ +d(\mathbf{x}, M), & \mathbf{x} \in R_M \\ -d(\mathbf{x}, M), & \mathbf{x} \in \Omega \backslash R_M \end{cases} \tag{1}$$

where $\mathbf{x} = (x, y)$ is the pixel location in Cartesian coordinates and $d(\mathbf{x}, M)$ denotes the minimum Euclidean distance from the pixel location $\mathbf{x}$ to the model M. We

formulate the segmentation problem as a joint MAP estimation problem:

$$\langle \Phi_M^*, L^* \rangle = \arg\max_{(\Phi_M, L)} P(\Phi_M, L|I) \tag{2}$$

where L is the set of the pixel labels, i.e., $L = \{\text{tumor, background}\}$, and I is the input image. Based on the graphical model of Ref. 15, the probability $P(\Phi_M, L|I)$ is decomposed into,

$$P(\Phi_M, L|I) = P(\Phi_M) \cdot P(I) \cdot P(L|\Phi_M) \cdot P(L|I) \tag{3}$$

where $P(I)$ is the image prior (Gaussian distribution), the likelihood $P(L|\Phi_M)$ is formulated as a softmax function,[15] while the model prior $P(\Phi_M)$ is a probabilistic expression of the model internal energy (smoothness term).[15] The remaining term $P(L|I)$ in Eq. (3) is estimated by using the discriminative CRF,[15,16] which can provide a smooth probability field L for the entire image.

The overall algorithm for the model evolution consists of the following steps:

(i) Model initialization and learning of the tumor texture using the model interior: discriminative estimation of $P(L|I)$, assuming conditional independence between the pixels.
(ii) Estimation of the probability field $P(L|I)$ using the discriminative CRF to capture local pixel dependences and the probability field calculated in (i).
(iii) Evolution of the model within a band around it, based on Eq. (2).
(iv) For the new position of the model, update the model interior (tumor) statistics and repeat the steps (ii)–(iv).

3. Results and Discussion

3.1. *Imaging normal mouse and rat retina*

We first performed experiments on the eyes of a mouse free of tumor and a Wistar rat with normal retina to assess the capability of the OCT system in imaging retinal structures of small animals. 3D OCT datasets were acquired on the central area of the retina for both animals. The results are shown in Fig. 2A and 2B, respectively. The cross-sectional images are located distal to the optic disc. The images are displayed in grayscale: darker reading corresponding to lower backscattering and brighter reading to higher backscattering. The displayed depth is 0.73 mm after corrected with the refractive index of the retina. The images consist of 512 axial scans. All the intra-retinal layers can be identified in the images. The overall quality of the OCT images is high.

3.2. *Alignment performance of the animal positioning system*

The animal positioning system was tested on a mouse eye free of tumor. The animal was restrained in a tube and placed on the animal positioning system with the eye centered at the intersection of the two rotational axes, which was achieved by fine

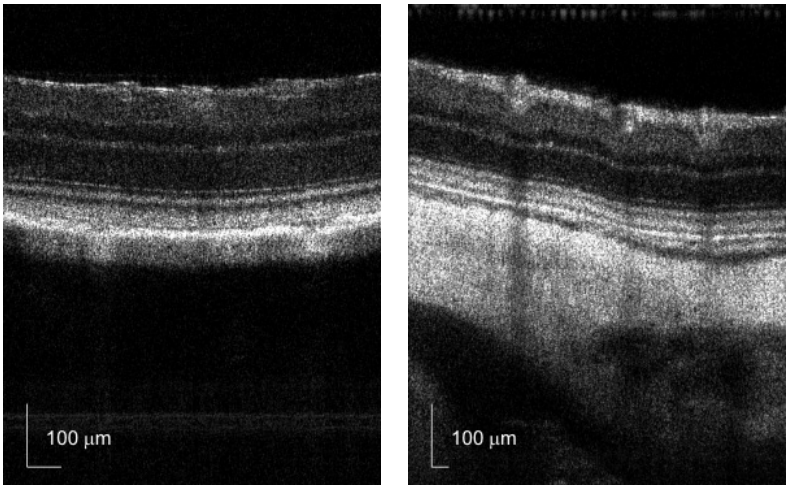

(A) (B)

Fig. 2. Cross-sectional OCT retinal images of a transgenic mouse (A) and a Wistar rat (B) distal to the optic disc. All the intraretinal layers can be recognized in the cross-sectional images.

adjustment of the X, Y and Z translation stages. We first adjust the animal so that the optic disc is imaged on the middle OCT image in the real-time display. We then record the readings of the rotational stages for roll and yaw as the original positions. We then successively rotated the positioning system along the roll and yaw directions separately and monitor the vertical positions (imaging depth) of the three real-time OCT images. Figure 3 shows the vertical position of the center of the retinal surface in the real-time OCT image at the middle of the scanned area for different rotational angles along the two rotational axes. The rotation range in

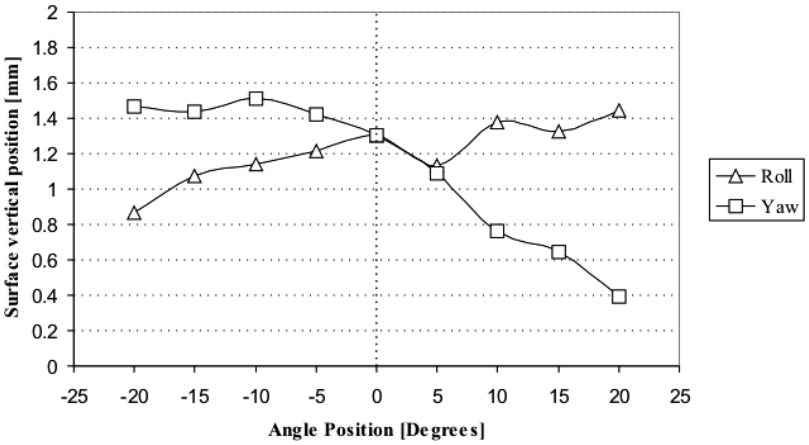

Fig. 3. Positions of the center of the retinal surface in the real-time OCT images for different rotational angles along the two rotational axes (roll and yaw).

the test for both rotational degrees of freedom is about $\pm 20°$. The tests showed that the OCT images of the mouse retina remain in the field of view of the OCT system within the rotation range of $\pm 20°$ for both rotational axes.

3.3. *In vivo quantitative monitoring tumor progression*

We tested our OCT system on the monitoring of retinal tumor growth in the mouse model of retinoblastoma by imaging the same tumor at 4 time points. With the guidance of the real-time OCT display and later on verified by the constructed OCT fundus image it was ensured that the same tumor was covered for each time point. In each OCT B-scan image the retinal tumor boundary was automatically segmented. The volume of the tumor at each time point was calculated by counting the number of voxels the tumor covered. Figure 4 shows four OCT cross-sectional images located at the same position on the registered fundus images acquired at different time points. The tumor was located in the superior region of the retina distant to the optic disc. For each time point two partially overlapped areas of the retina were scanned, one of which covered the tumor while the other was close to the optic disc. The two scanned areas can be registered according to the blood vessel patterns in the OCT fundus images (Fig. 4). The tumor can be clearly recognized in the OCT cross-sectional images as a highly backscattering region growing over time. The displayed image depth of the images is 650 pixels corresponding to 0.73 mm.

Figure 5 shows an example of the tumor segmentation using our method. Figure 5A shows the initial OCT image where the tumor is located inside the yellow

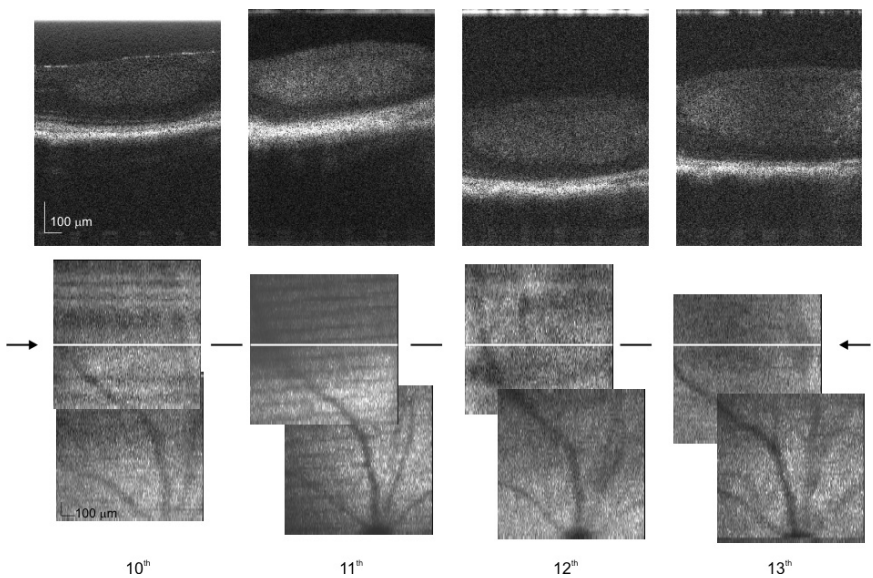

Fig. 4. OCT cross-sectional images located at the same position on the registered fundus images and acquired at different time points: 10^{th}, 11^{th}, 12^{th}, and 13^{th} week of the age, respectively.

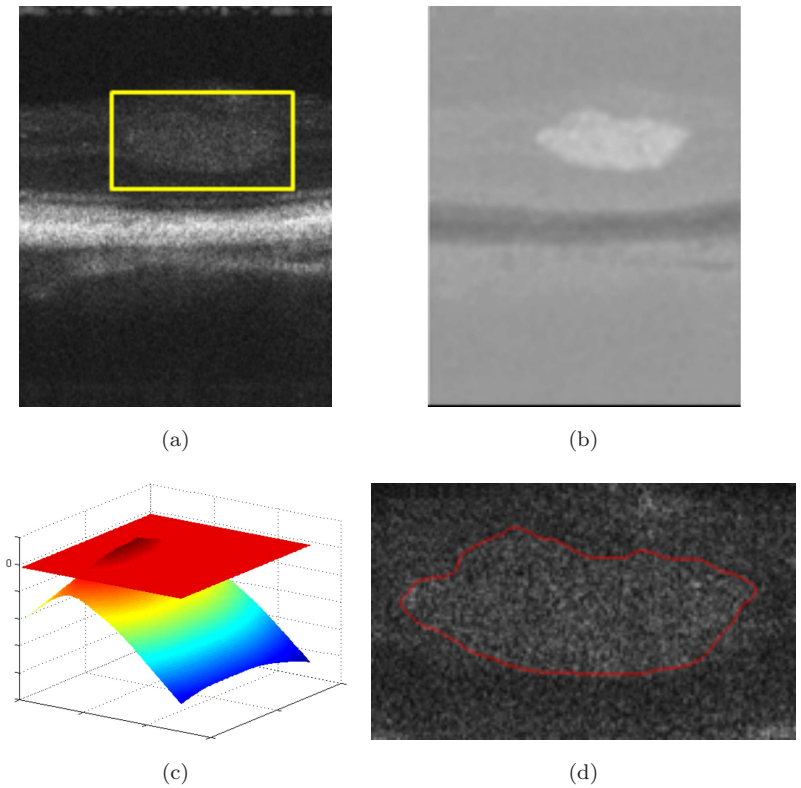

Fig. 5. Segmentation of retinal tumors using our CRF-driven deformable model: A) original image with the yellow box indicating the location of the tumor. B) Final probability field: brighter regions correspond to high probabilities, while darker regions correspond to low probabilities of the image regions belonging to the tumor. C) The final solution of the deformable model: the surface corresponds to the model's shape representation (distance function): the tumor boundary D) is estimated as the cut of the model representation (surface) with the zero level (red plane in C)).

box. Figure 5B shows the final probability field $P(L|I)$ that the discriminative CRF estimated at the last iteration of the model evolution. From this probability field we obtain the region labels {tumor, background} L^* of Eq. (2): the brighter regions of the image correspond to high probability of belonging to the tumor. Figure 5C shows the final configuration of the model Φ^*_M of Eq. (2), as represented by the distance function of Eq. (1). The tumor boundary of Fig. 5D is then obtained as the cut of the surface Φ^*_M with the zero level (red plane of Fig. 5C).

We calculated the tumor volume with the voxel counting method applied to the segmented OCT images. The 3D OCT image covers a retinal volume of $1 \times 1 \times 1.15$ (horizontal $\times$ vertical $\times$ depth) mm^3 consisting of $512 \times 128 \times 1024$ voxels, where the imaging depth has been corrected by the refractive index of the mouse retina. We calculated the volume for each voxel of the image as 17.1 μm^3. By counting the total number of voxels confined by the segmented boundaries, which has been done

Table 1. Tumor volume calculated from OCT images as described in the text.

Time stage [week]	Voxel counting [number of voxels]	Tumor volume [mm^3]
10	1532829	0.0262
11	2912422	0.0498
12	4085199	0.0699
13	> 5800000	> 0.0992

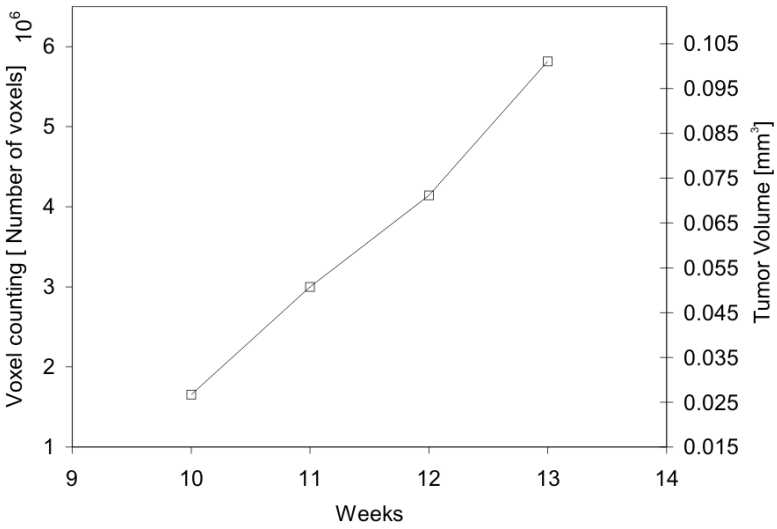

Fig. 6. Progressive growth of the tumor size in the retina of a $LH_{BETA}T_{AG}$ mouse model. Tumor volume was measured at 4 different stages of the disease from the 10th week to the 13th week of age. Each point represents the tumor volume in number of voxels and in mm^3.

automatically by the software, the total volume of the tumor was calculated. Tumor volumes were calculated for the four stages of the disease. The calculated values are shown in Table 1 and plotted in Fig. 6. It is important to note that during 4 weeks of observation the measured tumor volumes increased almost linearly over time. Although at 13 weeks of age the tumor region extended outside the imaging area (Fig. 4) its measured partial volume is larger than the values calculated in the previous weeks.

4. Conclusion

We have developed a spectral domain optical coherence tomography system for noninvasive *in vivo* three-dimensional imaging of retinal tumor in transgenic mouse models. The imaging device was combined with an advanced animal positioning system, which allows the operator to rapidly locate and shift the area of interest on the retina. Therefore, it solves the problem of long examination time in searching tumor at the beginning of a study cycle. In fact, our system allowed locating retinal tumors in less than 2 minutes including the time to align the mouse

on the positioning system. The animal aligning system played a crucial role in high throughput longitudinal studies. An algorithm for fully automatic segmentation of tumor boundaries was developed and used in quantitative monitoring the tumor growth in a transgenic mouse model of retinoblastoma. The OCT system and the segmentation algorithm were successfully tested on the mouse eye for the first time.

Acknowledgments

The authors thank for scientific and technical contributions from Hinda Boutrid, Robert Knighton, Giovanni Gregori, Xiangrun Huang, Randolph Manriquez, William Lee, and Izuru Nose (all from Bascom Palmer Eye Institute). This study is supported in part by the NIH (NEI grant R01 EY01629), the NEI P30 Core Grant Ey014801 and U.S. Army Medical Research and Materiel Command (USAMRMC) grant W81XWH-07-1-0188.

References

1. A. Tamboli, M. J. Podgor and J. W. Horm, "The incidence of retinoblastoma in the United States: 1974 through 1985," *Archives Ophthalmology* **108**, 128–132 (1990).
2. T. W. Pendergrass, S. Davis, "Incidence of retinoblastoma in the United States," *Archives Ophthalmology* **98**, 1204–1210 (1980).
3. D. Huang, E. A. Swanson, C. P. Lin, J. S. Schuman, W. G. Stinson, W. Chang, M. R. Hee, T. Flotte, K. Gregory, C. A. Puliafito and J. G. Fujimoto, "Optical coherence tomography," *Science* **254**, 1178–1181 (1991).
4. A. F. Fercher, C. K. Hitzenberger, G. Kamp and S. Y. El-Zaiat. "Measurement of intraocular distances by backscattering spectral interferometry," *Optics Communications* **117**, 43–48 (1995).
5. Q. Li, A. M. Timmers, K. Hunter, C. Gonzalez-Pola, A. S. Lewin, D. H. Reitze, W. W. Hauswirth, "Noninvasive imaging by optical coherence tomography to monitor Retinal Degeneration in the mouse," *Investigative Ophthalmology & Visual Science* **42**, 2981–2989 (2001).
6. N. Horio, S. Kachi, K. Hori, Y. Okamoto, E. Yamamoto, H. Terasaki and Y. Miyake, "Progressive change of optical coherence tomography scans in retinal degeneration slow mice," *Archives Ophthalmology* **119**, 1329–1332 (2001).
7. I. Hartl, T. Ko, R. K. Ghanta, W. Drexler, A. Clermont, S. E. Bursell and J. G. Fujimoto, "In vivo ultrahigh resolution optical coherence tomography for the quantification of retinal structure in normal and transgenic mice," *Investigative Ophthalmology & Visual Science* **42**, S793, 2001 (ARVO Abstract #4252).
8. S. M. Shah, E. L. e Silva, Y. Salshin, S. F. Hackett, F. Woreta and P. A. Campochiaro, "Comparison of retinal thickness of mice retina with stratus OCT and histology," ARVO Abstract #2375, Fort Lauderdale (2004).
9. K. Kim, G. N. Maguluri, M. Puorishaag, Y. Umino, R. B. Barlow, J. F. De Boer, "Optical coherence tomography for mouse retinal imaging," ARVO Abstract #2923, Fort Lauderdale (2006).
10. V. J. Srinivasan, T. H. Ko, M. Wojtkowski, M. Carvalho, A. Clermont, S. E. Bursell, Q. H. Song, J. Lem, J. S. Duker, J. S. Schuman and J. G. Fujimoto, "Noninvasive volumetric imaging and morphometry of the rodent retina with high-speed, ultra

high-resolution optical coherence tomography," *Investigative Ophthalmology & Visual Science* **47**, 5522–5528 (2006).
11. M. Ruggeri, H. Wehbe, S. Jiao, G. Gregori, M. E. Jockovich, A. Hackam, Y Duan and C.A. Puliafito, "In vivo three-dimensional high-resolution imaging of rodent retina with spectral-domain optical coherence tomography," *Investigative Ophthalmology & Visual Science* **48**, 1808–1814 (2007).
12. J. J. Windle, D. M. Albert and J. M. O'Brien, "Retinoblastoma in transgenic mice," *Nature* **343**, 665–669 (1990).
13. S. Remtulla and P. E. Hallett, "A schematic eye for the mouse, and comparisons with the rat," *Vision Research.* **25**, 21–31 (1985).
14. S. Jiao, R. Knighton, X. Huang, G. Gregori and C. Puliafito, "Simultaneous acquisition of sectional and fundus ophthalmic images with spectral-domain optical coherence tomography," *Optics Express* **13**, 444–452 (2005) http://www.opticsinfobase.org/abstract.cfm?URI=oe-13-2-444
15. G. Tsechpenakis and J. Wang, "CRF-based segmentation of human tear meniscus obtained with optical coherence tomography," IEEE International conference on Image Processing (ICIP), San Antonio, TX, September 2007.
16. G. Tsechpenakis and D. Metaxas, "CRF-driven Implicit Deformable Model," IEEE Conference on Computer Vision and Pattern Recognition (CVPR), Minneapolis, MN, June 2007.
17. G. Tsechpenakis, J. Wang, B. Mayer and D. Metaxas, "Coupling CRFs and deformable models for 3D Medical Image Segmentation," IEEE Mathematical Methods in Biomedical Image Analysis, International conference on Computer Vision (ICCV), Rio de Janeiro, Brazil, Oct. 2007.